

## Ink-jet printing of carbon nanotube thin film transistors

P. Beecher, P. Servati,<sup>a)</sup> A. Rozhin, A. Colli, V. Scardaci, S. Pisana, T. Hasan, A. J. Flewitt, J. Robertson, and G. W. Hsieh

*Department of Engineering, University of Cambridge, Cambridge, CB3 0FA, United Kingdom*

F. M. Li

*Electrical and Computer Engineering, University of Waterloo, Waterloo, Ontario, N2L 3G1, Canada*

A. Nathan

*London Centre for Nanotechnology, University College London, London, WC1H 0AH, United Kingdom*

A. C. Ferrari<sup>b)</sup> and W. I. Milne

*Department of Engineering, University of Cambridge, Cambridge, CB3 0FA, United Kingdom*

(Received 9 January 2007; accepted 10 July 2007; published online 27 August 2007)

Ink-jet printing is an important process for placing active electronics on plastic substrates. We demonstrate ink-jet printing as a viable method for large area fabrication of carbon nanotube (CNT) thin film transistors (TFTs). We investigate different routes for producing stable CNT solutions (“inks”). These consist of dispersion methods for CNT debundling and the use of different solvents, such as *N*-methyl-2-pyrrolidone. The resulting printable inks are dispensed by ink-jet onto electrode bearing silicon substrates. The source to drain electrode gap is bridged by percolating networks of CNTs. Despite the presence of metallic CNTs, our devices exhibit field effect behavior, with effective mobility of  $\sim 0.07$  cm<sup>2</sup>/V s and ON/OFF current ratio of up to 100. This result demonstrates the feasibility of ink-jet printing of nanostructured materials for TFT manufacture.

© 2007 American Institute of Physics. [DOI: [10.1063/1.2770835](https://doi.org/10.1063/1.2770835)]

### I. INTRODUCTION

The recent developments in plastic electronics are expected to revolutionize the electronics industry.<sup>1–6</sup> This will allow for a variety of applications to be envisaged, not attainable using conventional silicon chips because of their rigidity and limited size. Ink-jet printing is one of the most promising techniques for inexpensive large area fabrication of plastic electronics.<sup>2</sup> In fact, a range of electronic and optoelectronic components can be printed on plastic substrates, i.e., transistor circuits,<sup>1–5</sup> photovoltaic films,<sup>6</sup> organic light-emitting diodes (OLEDs),<sup>1,7</sup> and displays.<sup>1</sup> Within this field, much research has been devoted to the study of organic semiconductors, due to their compatibility with plastic substrates, along with their routine solution processability.<sup>8</sup> Many groups have fabricated organic thin film transistors (TFTs) by a variety of methods, including ink-jet printing.<sup>2,9–13</sup> Although organic TFTs often exhibit reasonably good ON/OFF current ratios, attempts to improve their low mobilities (typically  $< 0.1$  cm<sup>2</sup>/V s), poor air stability, and limited lifetime<sup>8</sup> remain a subject of ongoing research.

Several groups have recently considered alternative approaches, and have harnessed the electronic properties of materials such as carbon nanotubes (CNTs) in addressing this problem.<sup>14–21</sup> Experiments have been conducted using CNT/P3HT composite solutions spin-coated onto electrode-bearing substrates.<sup>14</sup> A 60-fold enhancement in mobility compared to that for pristine P3HT layers was reported (up to  $0.2$  cm<sup>2</sup>/V s). Pure CNT TFTs fabricated by elastomeric

stamp printing<sup>15</sup> and from as-grown CNT networks<sup>16</sup> have produced promising results, with device mobilities  $> 10$  cm<sup>2</sup>/V s. However, solution phase deposition processes have, so far, not given such good devices.<sup>17–20</sup> Pure CNT devices have been fabricated by means of a tilted drop casting technique, which promotes CNT alignment.<sup>17</sup> Although these films exhibit excellent current carrying capability, TFTs have very low ON/OFF ratios ( $< 3$ ), owing to the presence of metallic CNTs in the dense films. Devices have also been fabricated from CNTs by dissolving CNT-filled membranes after attachment of the membranes to substrates, with the aim of investigating the behavior around the metallic percolation threshold.<sup>18</sup> However, it was reported that TFT performance was compromised even below the percolation threshold of metallic CNTs. A spray coating technique has also been applied to the fabrication of CNT TFTs.<sup>19,20</sup> Low density films, though not with very high current carrying capability, were reported with ON/OFF ratios of five orders of magnitude.<sup>19</sup> CNT networks drop cast on flexible substrates, with spray coated CNT gate layers, have produced devices with mobilities of  $1$  cm<sup>2</sup>/V s and ON/OFF ratios of  $100$ .<sup>20</sup>

In comparison to other solution phase methods, ink-jet printing holds greater promise as a means of device integration, as it offers targeted film deposition, and is suitable for industrial-scale production. Ink-jet printing of conducting films of CNTs was recently reported using a commercial desktop ink-jet printer,<sup>21</sup> suggesting the viability of ink-jet technology as a means of depositing nanostructured materials for a variety of applications. In Ref. 21, thick electrically conductive mats of randomly oriented CNTs were fabricated by multiple ( $> 30$ ) prints over the same pattern. These

<sup>a)</sup>Also at: Electrical and Computer Engineering Dept., University of British Columbia, Vancouver, V6T 1Z4, Canada.

<sup>b)</sup>Corresponding author. Electronic mail: [acf26@eng.cam.ac.uk](mailto:acf26@eng.cam.ac.uk)

tangled networks exhibited reasonably low sheet resistance ( $\sim 40$  k $\Omega$ /square), but no field effect behavior.

In this article, we report fabrication of CNT TFTs by ink-jet printing. We investigate dispersion of CNTs in solutions suitable for ink-jet printing, and monitor the long-term stability of such solutions. Ink-jet printing of these solutions can be carried out on a variety of substrates including glass, Si, indium tin oxide, and also plastic substrates, whose flexible properties are crucial for the many applications considered for this technology. The electrical characteristics of CNT TFTs are evaluated in terms of field effect mobility and ON/OFF ratio to identify the underlying mechanisms governing their behavior.

## II. EXPERIMENT

Single-wall HiPCO CNTs (Carbon Nanotechnologies, Inc.) are dispersed in *N*-methyl-2-pyrrolidone (NMP), which has been observed experimentally to be a good solvent for CNTs.<sup>22–25</sup> The HiPCO CNTs used are typically on the order of 1  $\mu\text{m}$  in length and 1 nm in diameter.<sup>26</sup> Typical CNT concentrations prepared are on the order of 0.1–0.2 mg/mL. Sonication is carried out in a 200 W, 20 kHz sonication bath (Bioruptor; Diagenode) for 1 h, before intense ultracentrifugation for 30 min at 30 000 rpm (Beckman, Optima MAX-E). The top fraction ( $\sim 50\%$ ) is carefully removed using a pipette, and the rest of the solution is discarded. Prior to ink-jet printing, solutions are filtered using 0.7  $\mu\text{m}$  filter paper (Whatman), in order to ensure that very large aggregates of CNTs are not used in the ink-jet nozzles.

Ink-jet printing is performed using an Autodrop ink-jet dispensing system featuring piezoelectric dispenser heads with 50  $\mu\text{m}$  diameter nozzles (Microdrop GmbH). The ink-jet nozzles are piezo-driven, from which drops are deposited by a voltage pulse. The voltage level and the duration of the pulse are used to control the drops emitted from the nozzle. The voltage level typically used in this research is on the order of 150–200 V, with pulse duration of 37  $\mu\text{s}$ . Drops are generally dispensed at a frequency of 50 Hz, although that can be raised considerably using this system, up to 2 kHz. The limiting factor for an ink is its viscosity, as inks of high viscosity (approaching 10 MPa s) cannot be printed at higher frequencies. The printing speed, i.e., the speed of the nozzle head between device locations, is on the order of 10 mm/s, but this could be increased to 125 mm/s.

The resulting solutions are characterized by Raman spectroscopy, at 514, 633, and 785 nm, using a Renishaw micro-Raman 1000 spectrometer system. Ultraviolet/visible/infrared (UV/Vis/IR) absorption spectroscopy is performed with a Perkin Elmer Lambda 950 UV/Vis Spectrophotometer. Scanning electron microscopy (SEM) was carried out using a Philips XL30 SFESEM.

Transport measurements of CNT TFTs are performed using interdigitated gold electrodes with interelectrode gaps of  $\sim 4$   $\mu\text{m}$ , fabricated by optical lithography on silicon wafers with an oxide thickness of  $\sim 150$  nm. Prior to ink-jet deposition, substrates are immersed in a solution of octadecyltrichlorosilane (OTS) in toluene for 15 min at 60  $^{\circ}\text{C}$  in order to prepare a hydrophobic self-assembled monolayer of OTS

on the surface. CNT solutions are then dispensed onto substrates in ambient conditions where the solvent is allowed to evaporate slowly, followed by annealing at  $\sim 140$   $^{\circ}\text{C}$  to remove residual NMP. Electrical measurements are carried out using a Keithley Semiconductor Characterization System (SCS) 4200. Medium integration and a delay of 200 ms are used to ensure that no transient instabilities in the current occur.

## III. RESULTS AND DISCUSSION

Given that it is intended to dispense nanostructured materials by means of ink-jet, it is vital to be able to achieve a highly effective dispersion of these materials in solution. Thus, we first study the dispersion of single-wall HiPCO CNTs in a variety of commonly used organic solvents, e.g., dimethylformamide, toluene, chloroform, acetone, anisole, methanol, and NMP. Following synthesis, CNTs tend to form dense clumps, and it requires a significant amount of coercion in order to disperse them effectively.<sup>27</sup> For this reason, we employ a high power sonication and ultracentrifugation apparatus. It was observed that NMP, a dipolar aprotic solvent, is a very effective solvent for producing CNT solutions.<sup>22–25</sup> The combination of the excellent solvency properties of NMP and intense dispersion techniques allows for the preparation of quite stable solutions of CNTs without the need for a surfactant, which is usually necessary for long-term stability of CNT dispersions.<sup>25</sup> Other notable characteristics of NMP are its high boiling point (202  $^{\circ}\text{C}$ ), and heat of vaporization (54.5 kJ/mol).<sup>28</sup> Droplets dispensed by ink-jet, which are in the sub-nano-liter range,<sup>29</sup> may thus take several hours to completely evaporate at room temperature.

Concentrations of CNTs in NMP are estimated by examining the intensity of the absorption peaks between 550 and 1320 nm of various fractions of CNT solution obtained from the centrifugation and filtration processes, and also the sonicated solution containing the original concentration, which is known; see Fig. 1.<sup>22,30</sup> Absorption spectra are obtained sequentially with the same reference used in each case, in order for estimates of the CNT concentration to be as accurate as possible.<sup>25</sup> To estimate CNT concentration in the various dispersions, the absorption coefficient ( $\alpha$ ) of HiPCO CNTs in NMP must be measured. For this purpose, CNT dispersions of different known concentrations ranging from 0.06 to 0.003 mg/mL are investigated using UV-Vis absorption spectroscopy following ultrasonic treatment only.<sup>25</sup> The absorption coefficient of HiPCO CNTs in NMP at 740 nm is found to be  $\sim 4300$  mL  $\text{mg}^{-1}$   $\text{m}^{-1}$  using the Beer–Lambert law. Using this value for  $\alpha$ , we obtain values for the concentration of CNTs in NMP after ultracentrifugation ( $\sim 0.012$  mg/mL). Prior to ink-jet printing, our solutions are filtered to remove larger agglomerates, and this reduces the concentration even further to approximately 0.003 mg/mL. Solutions obtained after ultracentrifugation and filtration, which do not include surfactant, remain stable over long periods, with precipitation of large agglomerates not being observable to the eye for periods of up to a few months. Fig. 2(a) shows a photograph of our CNT solution in NMP. Note

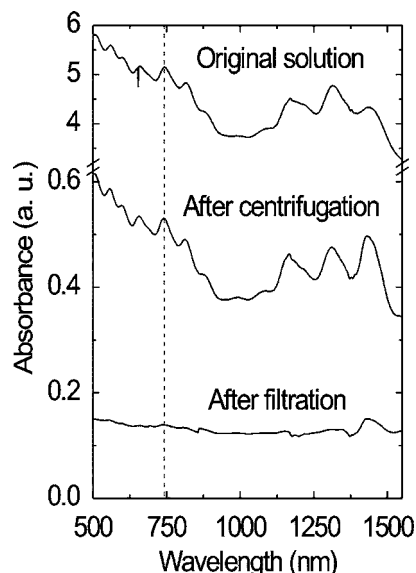


FIG. 1. Absorption spectra of original solution of CNTs, as well as fractions removed following ultracentrifugation and filtering. Concentration estimated at 740 nm, where there is a well-defined peak for each fraction.

that the solution is almost completely transparent following the filtering process to remove the larger clumps of agglomerated CNTs.

Within the dispenser head of the ink-jet system, there is a  $5\ \mu\text{m}$  filter to prevent large particles from clogging the ink-jet nozzles. This then requires very good dispersion of CNTs in solution in order to enable ink-jet of CNT droplets. HiPCO CNTs are typically on the order of  $1\ \mu\text{m}$  in length and  $1\ \text{nm}$  in diameter, although even in the best dispersed solutions there exists bundles/ropes containing a small number of CNTs, owing to van der Waals forces.<sup>25,27</sup> Large agglomerates of these CNTs therefore lead to clogging of the ink-jet nozzles. Aggressive dispersion methods, followed by filtering of solutions, enable the routine deposition of CNT films using this ink-jet system. Large-scale arrays and tracks

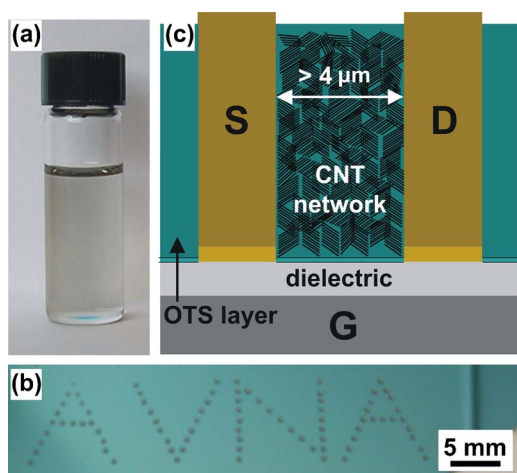


FIG. 2. (Color online) (a) Photograph of solution of HiPCO CNTs dissolved in NMP. (b) Photograph of an example of drops printed in a pattern using the ink-jet system. Drops, with an approximate diameter of  $0.5\ \text{mm}$ , are comprised of 50 small drops deposited by ink-jet at each dropping site. (c) Schematic of CNT TFT device structure. There is a layer of OTS prepared on the substrate prior to the ink-jet deposition of CNTs.

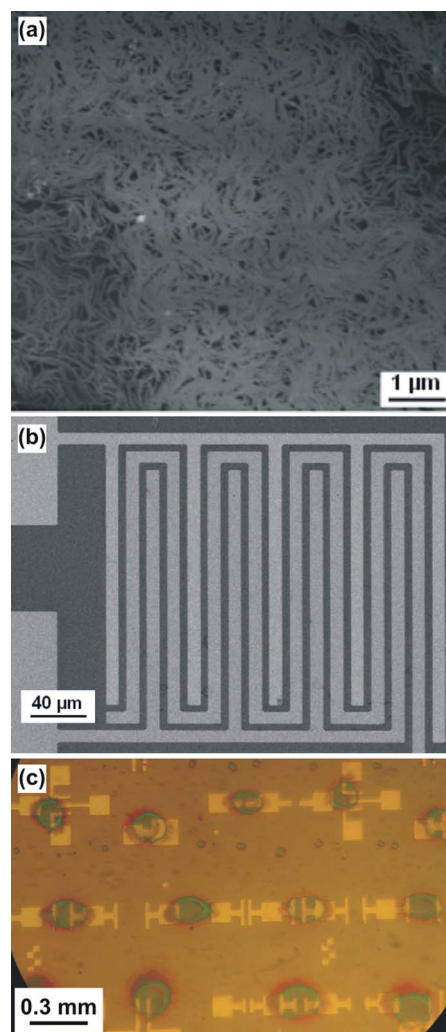


FIG. 3. (Color online). (a) SEM image of a CNT film, (b) SEM of typical electrode structure used, and (c) optical micrograph of devices fabricated by ink-jet. Here the channels are composed of organic polymer, which aids visualization.

can easily be formed, so there is scope for producing a variety of different device patterns. Fig. 2(b) shows an example of a pattern that can be produced by this ink-jet system. Drops dispensed from a nozzle of diameter  $50\ \mu\text{m}$  tend to spread to approximately  $100\ \mu\text{m}$  on a modified substrate. Once the solvent is evaporated, the remaining layer of CNTs is observed to have contracted to a diameter of  $20\text{--}40\ \mu\text{m}$ .

Even though large-scale bulk aggregation is not observed to occur in solutions of CNTs in NMP over a short time frame, it is observed from SEM images that aggregation at a microscopic level does occur within days of preparation of a solution. Week-old solutions, though printable, do not form arrays on substrates, but are deposited as aggregates. As a consequence, solutions of CNTs are not kept in the print head following printing, which is instead flushed with solvent or deionized water. This precaution is taken to ensure that repeated printing can be performed without the occurrence of clogging. Fig. 3(a) shows a SEM image of HiPCO CNTs deposited by ink-jet on a Si substrate. The coverage of CNTs is quite dense, given the transparency of the solution prior to ink-jet deposition, and therefore there is a strong

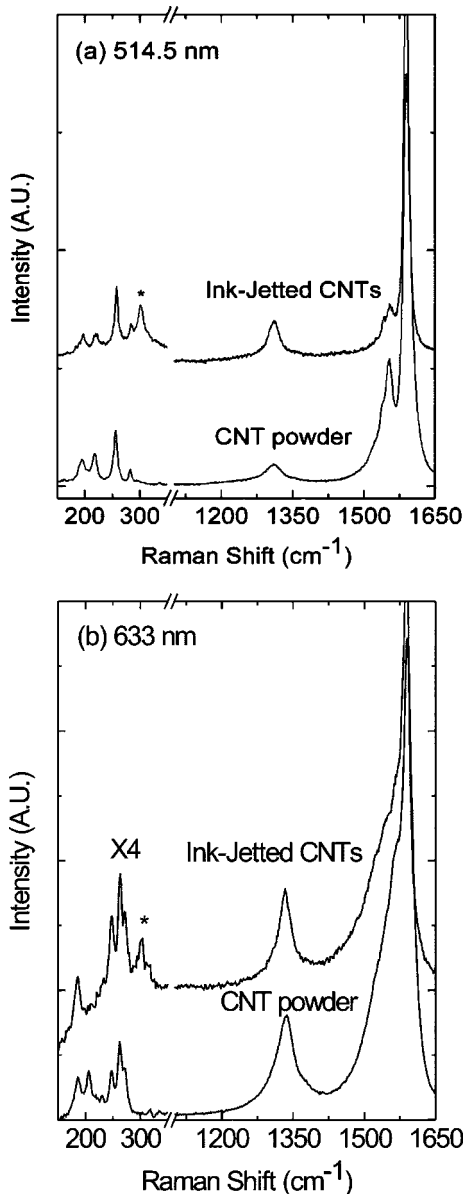


FIG. 4. Raman spectra of HiPCO CNT powder and CNT film deposited on Si substrates by ink-jet measured at 514 and 633 nm, respectively. Note that the peak indicated by an asterisk (\*) is due to the silicon substrate and is not a RBM (Ref. 31).

likelihood of forming a percolating network of CNTs. Fig. 3(b) shows a SEM of a device structure, in which the electrode gap is bridged by just such a network of CNTs, whereas Fig. 3(c) shows an optical micrograph of an array of devices fabricated by ink-jet. Here, for the purposes of visualization of films deposited by ink-jet, the printed material is composed of organic polymer.

Raman spectroscopy is used to monitor our CNTs throughout all processing steps; see Fig. 4. The diameter of single wall carbon nanotubes (SWNT) can be derived from the radial breathing mode (RBM) frequency:  $d = C_1 / (\omega_{\text{RBM}} - C_2)$ , where  $C_1 = 214.4 \text{ cm}^{-1}$  and  $C_2 = 18.7 \text{ cm}^{-1}$ ,<sup>32</sup> combined with the Kataura plot<sup>33</sup> and the known excitation energy. We stress that due to the cutoff of our notch filter, we cannot detect CNT diameters  $> 2 \text{ nm}$ . Note as well that a variety of different  $C_1$  and  $C_2$  values have been

proposed,<sup>32,34</sup> but their precise value is only critical for chirality assignment. Here we only consider the CNT diameter distribution and establish if they are metallic or semiconducting; thus the precise  $C_1$  and  $C_2$  are not critical. The starting material has a diameter ranging from 0.8 to 1.4 nm. It is also composed of a mixture of metallic and semiconducting nanotubes, as can be seen both from the RBM positions and the typical metallic shape of the  $G^-$  peak for 633 nm and semiconducting shape at 514.5 nm.<sup>35-37</sup> The Raman spectra of the samples deposited on the substrate are remarkably similar to those of the starting material in terms of diameter distribution, as shown in Fig. 4 for the excitation wavelengths considered. This indicates that the dispersion process does not modify the character of the starting material, unlike other processes reported in literature.<sup>38</sup>

Having demonstrated efficacy of dispersion and ink-jet of CNTs, we now consider the properties of devices built incorporating ink-jetted CNTs. Several techniques have been reported for successful organization of one-dimensional nanowires and nanotubes into films, including the Langmuir-Blodgett technique,<sup>39,40</sup> lithographically directed fluidic assembly,<sup>41</sup> electric-field-assisted assembly,<sup>42</sup> fluidic alignment,<sup>17,43</sup> surface modification for guided assembly,<sup>44</sup> and electrophoresis.<sup>45,46</sup> For our devices, we employ surface modification to try and achieve large-scale preferential alignment of CNTs between electrodes. To form a hydrophobic self-assembled monolayer, we use OTS, which is typically used in the alignment of lamellae of organic semiconductors.<sup>47,48</sup> OTS surface treatment can produce domains of well-stacked lamellas of semiconducting molecules, which facilitates efficient charge transport between adjacent lamellas.<sup>49,50</sup> A schematic of the CNT film deposited on a modified substrate, in which the film is composed of domains of aligned CNTs, is shown in Fig. 2(c). We see regions where CNTs are weakly aligned [Fig. 3(a)], which we surmise will enhance percolation in our assemblies.

Output characteristics of an inkjet-printed CNT TFT biased at different gate voltages ( $V_G = -6, -4, -2, 0, 2, 4,$  and  $6 \text{ V}$ ) is depicted in Fig. 5(a). For each gate voltage, the drain voltage is swept from 0 to  $-8 \text{ V}$  in steps of  $-0.25 \text{ V}$ . Increasing drain voltage beyond this value leads to significantly lower current. For the device shown in Fig. 5, an initially higher current was measured than is reported here, before the current level decreased. It is assumed that this transition is a result of the burning of some of the metallic CNTs, but it is not easy to remove them completely as within this film there is a random mixture of CNTs with no single tubes bridging the contacts. Consequently, by raising the voltage, it is possible to burn conduction paths that contain a relatively high number of metallic CNTs. But for the conduction paths where only a few metallic CNTs are present, the voltage drops mainly across the semiconducting CNTs that shield the metallic ones. Despite this, the characteristics still clearly resemble those of a field effect transistor, where drain current increases and saturates as the negative drain voltage is increased. For higher negative gate bias, the current level increases as expected for a  $p$ -type transistor.<sup>15-20</sup>

Fig. 5(b) shows a logarithmic plot of the drain current as

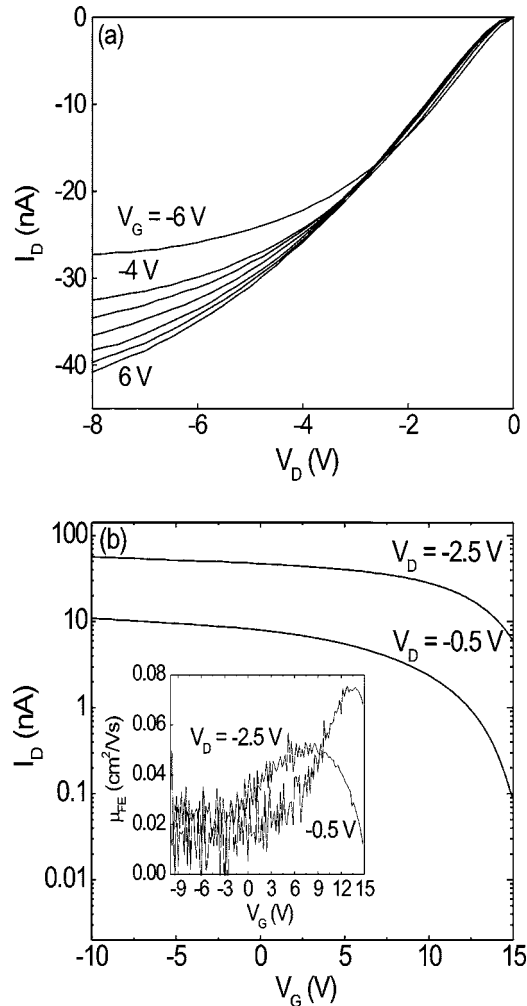


FIG. 5. (a) Output characteristics of ink-jet printed CNT TFT for different gate biases. (b) Transfer characteristics of the same TFT for  $V_D = -0.5$  and  $-2.5$  V. Inset: mobility as a function of gate voltage.

a function of gate voltage for different drain biases. For each drain bias, the gate voltage is swept from 15 V to  $-10$  V in steps of  $-0.2$  V. The drain current increases as the gate voltage decreases, due to the field effect exhibited by semiconductor CNTs in the film. The minimum drain current is relatively high and depends on the drain bias. At  $V_D = -0.5$  V, an ON/OFF ratio of over two orders of magnitude is observed. However, at  $V_D = -2.5$  V, the gate is less effective in turning off the current, with the ON/OFF ratio reduced to  $\sim 6$ . This is due to the fact that there are metallic CNTs in the overlap of the film with the gold contacts (as shown in the Raman spectra of Fig. 4), which makes it impossible to eliminate carrier injection completely. At lower positive gate voltages ( $V_G < 10$  V), the drain current increases more slowly, again due to the limiting effect of a carrier injection barrier at the gold contacts. This influence can be viewed more clearly from the inset of Fig. 5(b), which shows the effective mobility extracted from the slope of the current voltage characteristics according to

$$\mu_{FE} = L/(WC_i V_D) dI_D/dV_G \quad (1)$$

where  $L$  is the channel length of the device,  $W$  is the channel width, and  $C_i$  is the gate dielectric capacitance

( $\sim 23$  nF/cm<sup>2</sup>). At  $V_D = -0.5$  V, the effective mobility is low due to the limited injection from the contacts. However, as we increase the drain voltage to  $-2.5$  V, the contacts do not influence the extracted mobility for  $11$  V  $< V_G < 14$  V, where a peak effective mobility of  $\sim 0.07$  cm<sup>2</sup>/V s is extracted. Reducing the gate voltage below 10 V degrades the effective mobility for both drain voltages possibly due to the same limiting effect of the gold contacts.

Thus, the mixture of metallic and semiconducting CNTs in our films is responsible for our high OFF current and low ON/OFF ratio. The metallic CNTs (with  $\sim 50$  times higher field-independent conductance in comparison to semiconducting ones)<sup>51</sup> act as a network of leakage paths that undermine the field effect characteristics of the TFTs.<sup>18</sup> Although our ON/OFF ratio (with a maximum of more than 100) is several orders of magnitude lower than that of amorphous silicon TFTs,<sup>7</sup> it constitutes a significant improvement over previously reported values for CNT TFTs.<sup>17,18,20</sup> The OFF current and the level of gate control over current-voltage characteristics are crucial for TFT applications in displays and large area imagers, as it determines if the device acts as a reliable switch or transistor. CNT density and coverage is critical in determining the influence of the percolating network of metallic CNTs.<sup>18</sup> A CNT density that is higher than a threshold ( $\Phi_C$ ) for formation of a percolation path of metallic CNTs undermines the semiconductor character of the film. Therefore, the CNT density should be lower than this threshold, but high enough to provide a percolation path for carrier hopping between semiconductor CNTs. In comparison to previous reports, our higher ON/OFF ratio and lower OFF current can be attributed to the lower density of the CNT film that is formed on the surface, whose assembly is aided by the self-assembled monolayer.

As can be seen in the SEM micrograph of Fig. 3(a), the CNTs lie flat beside each other in a spaghetti form with semi-ordered domains.<sup>48,49</sup> The low density of the film can reduce the probability of linking metallic CNTs acting as a metallic percolation path, and consequently, decrease the metallic leakage. This is in contrast to thick and high density CNT films achieved by repeated printing<sup>21</sup> or other methods<sup>17</sup> that lead to higher apparent mobility but very low gate control, higher OFF current, and lower ON/OFF ratio. Although we believe thicker CNT films are advantageous in terms of delivering higher currents, inferior gate control limits the number of potential applications for such films, and rules them out for use as the channel material for TFTs.

It is important to note that the field-effect mobility is extracted from the slope of the current-voltage characteristics in the linear regime according to Eq. (1). As a result, the extracted field-effect mobility is only due to the percolating network of semiconducting CNTs. This is in contrast to the extraction of mobility from the magnitude of current based on channel length experiments, which results in high mobility values due to the contribution of both metallic and semiconducting CNTs. The observed peak mobility in our films is quite comparable to that of amorphous silicon and organic TFTs currently being used for large area electronics and flexible displays.<sup>7,8</sup> However, it is important to note that the mobility is much lower than that expected from ballistic car-

rier transport in CNTs, due to the fact that the limiting mechanism is carrier hopping between CNTs in a random percolating network.

Therefore, achieving an optimal CNT density in films is of great importance, whether to have higher current or to have better switching, and will be the focus of future investigations. Considering the likely trade-offs involved in the concentration of CNTs used, it is difficult to gauge an upper limits of this technology where desirable TFT device characteristics such as a large ON/OFF ratio are preserved. At present, the presence of metallic CNTs in these TFTs constitutes a drawback. However, the amount of semiconducting nanotubes could be controlled during preparation of the CNT solution<sup>38</sup> or by post-deposition treatment.<sup>52</sup> Future work will target the role of CNT concentration in affecting device characteristics. But we believe the present work demonstrates amply the feasibility of the ink-jet technique for dispensing CNTs in order to fabricate TFTs, with potential for a variety of other devices as well, such as photovoltaic films, OLEDs, etc.

Finally this technique can be easily implemented to other nanomaterials, such as semiconducting nanowires.<sup>53</sup>

#### IV. CONCLUSIONS

We have demonstrated the fabrication of CNT TFTs by means of ink-jet printing. Stable solutions of CNTs are formed without requiring any surfactant, and these can be easily dispensed without clogging the ink-jet nozzles. This, along with the electrical performance observed from our devices, demonstrates their viability for use in low cost ink-jet print manufacturing of TFTs. Further work will address the challenges associated with organic TFTs, where the transconductance and mobility could be improved by incorporating CNTs or nanowires into an organic semiconducting matrix, broadening the potential for plastic electronics.

#### ACKNOWLEDGMENTS

The authors thank Robert Murphy for useful discussions. This work was supported by Advance Nanotech, Inc., EPSRC Project Nos. GR/S97613 and EP/E500935/1, and the Ministry of Information and Communication, Republic of Korea (Project No. A1100-0602-0101). One of the authors (A.C.F.) acknowledges funding from the Royal Society and the Leverhulme Trust.

<sup>1</sup>S. R. Forrest, *Nature* (London) **428**, 911 (2004).

<sup>2</sup>H. Sirringhaus, T. Kawase, R. H. Friend, T. Shimoda, M. Inbasekaran, W. Wu, and E. P. Woo, *Science* **290**, 2123 (2000).

<sup>3</sup>Y. Sun, E. Menard, J. A. Rogers, H.-S. Kim, S. Kim, G. Chen, I. Adesida, R. Dettmer, R. Cortez, and A. Tewksbury, *Appl. Phys. Lett.* **88**, 183509 (2006).

<sup>4</sup>M. C. McAlpine, R. S. Friedman, and C. M. Lieber, *Proc. IEEE* **93**, 1357 (2005).

<sup>5</sup>M. Matters, D. M. de Leeuw, M. J. C. M. Vissenberg, C. M. Hart, P. T. Herwig, T. Geuns, C. M. J. M. M. J. Musaers, and C. J. Drury, *Opt. Mater.* **12**, 189 (1999).

<sup>6</sup>P. Peumans, S. Uchida, and S. R. Forrest, *Nature* (London) **425**, 158 (2003).

<sup>7</sup>P. Servati and A. Nathan, *Proc. IEEE* **93**, 1257 (2005).

<sup>8</sup>C. D. Dimitrakopoulos and P. R. L. Malenfant, *Adv. Mater.* **14**, 99 (2002).

<sup>9</sup>S. P. Li, D. P. Chu, C. J. Newsome, D. M. Russell, T. Kugler, M. Ishida, and T. Shimoda, *Appl. Phys. Lett.* **87**, 232111 (2005).

<sup>10</sup>A. C. Arias, S. E. Ready, R. Lujan, W. S. Wong, K. E. Paul, A. Salleo, M. L. Chabinyc, R. Apte, R. A. Street, Y. Wu, P. Liu, and B. Ong, *Appl. Phys. Lett.* **85**, 3304 (2004).

<sup>11</sup>Y. Wu, Y. Li, B. S. Ong, P. Liu, S. Gardner, and B. Chiang, *Adv. Mater.* **17**, 184 (2005).

<sup>12</sup>C. W. Sele, T. von Werne, R. H. Friend, and H. Sirringhaus, *Adv. Mater.* **17**, 997 (2005).

<sup>13</sup>M. Chason, P. W. Brazis, Jr., J. Zhang, K. Kalyanasundaram, and D. R. Gamota, *Proc. IEEE* **93**, 1348 (2005).

<sup>14</sup>X.-Z. Bo, C. Y. Lee, M. S. Strano, M. Goldfinger, C. Nuckolls, and G. B. Blanchet, *Appl. Phys. Lett.* **86**, 182102 (2005).

<sup>15</sup>S. H. Hur, C. Kocabas, A. Gaur, O. O. Park, M. Shim, and J. A. Rogers, *J. Appl. Phys.* **98**, 114302 (2005).

<sup>16</sup>E. S. Snow, J. P. Novak, P. M. Campbell, and D. Park, *Appl. Phys. Lett.* **82**, 2145 (2003).

<sup>17</sup>H. Ko and V. V. Tsukruk, *Nano Lett.* **6**, 1443 (2006).

<sup>18</sup>H. E. Unalan, G. Fanchini, A. Kanwal, A. Du Pasquier, and M. Chhowalla, *Nano Lett.* **6**, 677 (2006).

<sup>19</sup>A. Schindler, J. Brill, N. Fruehauf, J. P. Novak, and Z. Yaniv, *Physica E (Amsterdam)* **37**, 119 (2007).

<sup>20</sup>E. Artukovic, M. Kaempgen, D. S. Hecht, S. Roth, and G. Grüner, *Nano Lett.* **5**, 757 (2005).

<sup>21</sup>K. Kordás, T. Mustonen, G. Tóth, H. Jantunen, M. Lajunen, C. Soldano, S. Talapatra, S. Kar, R. Vajtai, and P. M. Ajayan, *Small* **2**, 1021 (2006).

<sup>22</sup>S. Giordani, S. D. Bergin, V. Nicolosi, S. Lebedkin, M. M. Kappes, W. J. Blau, and J. N. Coleman, *J. Phys. Chem. B* **110**, 15708 (2006).

<sup>23</sup>K. D. Ausman, R. Piner, O. Lourie, R. S. Ruoff, and M. Korobov, *J. Phys. Chem. B* **104**, 8911 (2000).

<sup>24</sup>J. L. Bahr, E. T. Mickelson, M. J. Bronikowski, R. E. Smalley, and J. M. Tour, *Chem. Commun.* **2**, 193 (2001).

<sup>25</sup>T. Hasan, V. Scardaci, A. G. Rozhin, P. H. Tan, W. I. Milne, and A. C. Ferrari, *J. Phys. Chem. C*, (in press), ASAP Article 10.1021/jp0723012 S1932-7447(07)02301-1.

<sup>26</sup>P. Nikolaev, M. J. Bronikowski, R. K. Bradley, F. Rohmund, D. T. Colbert, K. A. Smith, and R. E. Smalley, *Chem. Phys. Lett.* **313**, 91 (1999).

<sup>27</sup>M. J. O'Connell, S. M. Bachilo, C. B. Huffman, V. C. Moore, M. S. Strano, E. H. Haroz, K. L. Rialon, P. J. Boul, W. H. Noon, C. Kittrell, J. Ma, R. H. Hauge, R. B. Weisman, and R. E. Smalley, *Science* **297**, 593 (2002).

<sup>28</sup>D. R. Lide, *Handbook of Chemistry and Physics* 86th ed. (CRC Press, Boca Raton, FL, 2005).

<sup>29</sup>B. J. de Gans, P. C. Duineveld, and U. S. Schubert, *Adv. Mater.* **16**, 203 (2004).

<sup>30</sup>I. W. Chiang, B. E. Brinson, A. Y. Huang, P. A. Willis, M. J. Bronikowski, J. L. Margrave, R. E. Smalley, and R. H. Hauge, *J. Phys. Chem. B* **105**, 8297 (2001).

<sup>31</sup>P. A. Temple and C. E. Hataway, *Phys. Rev. B* **7**, 3685 (1973).

<sup>32</sup>H. Telg, J. Maultzsch, S. Reich, F. Hennrich, and C. Thomsen, *Phys. Rev. Lett.* **93**, 177401 (2004).

<sup>33</sup>H. Kataura, Y. Kumazawa, Y. Maniwa, I. Umezu, S. Suzuki, Y. Ohtsuka, and Y. Achiba, *Synth. Met.* **103**, 2555 (1999).

<sup>34</sup>A. Jorio, C. Fantini, M. A. Pimenta, R. B. Capaz, G. Samsonidze, G. Dresselhaus, M. S. Dresselhaus, J. Jiang, N. Kobayashi, A. Grüneis, and R. Saito, *Phys. Rev. B* **71**, 075401 (2005).

<sup>35</sup>M. A. Pimenta, A. Marucci, S. A. Empedocles, M. G. Bawendi, E. B. Hanlon, A. M. Rao, P. C. Eklund, R. E. Smalley, G. Dresselhaus, and M. S. Dresselhaus, *Phys. Rev. B* **58**, R16016 (1998).

<sup>36</sup>M. Lazzeri, S. Piscanec, F. Mauri, A. C. Ferrari, and J. Robertson, *Phys. Rev. B* **73**, 155426 (2006).

<sup>37</sup>S. Piscanec, M. Lazzeri, J. Robertson, A. C. Ferrari, and F. Mauri, *Phys. Rev. B* **75**, 035427 (2007).

<sup>38</sup>M. S. Arnold, A. A. Green, J. F. Hulvat, S. I. Stupp, and M. C. Hersam, *Nat. Nanotechnol.* **1**, 60 (2006).

<sup>39</sup>D. Whang, S. Jin, Y. Wu, and C. M. Lieber, *Nano Lett.* **3**, 1255 (2003).

<sup>40</sup>X. Li, L. Zhang, X. Wang, I. Shimoyama, X. Sun, W.-S. Seo, and H. Dai, *J. Am. Chem. Soc.* **129**, 4890 (2007).

<sup>41</sup>J. A. Liddle, Y. Cui, and P. Alivisatos, *J. Vac. Sci. Technol. B* **22**, 3409 (2004).

<sup>42</sup>K. M. Ryan, A. Mastroianni, K. A. Stancil, H. Liu, and A. P. Alivisatos, *Nano Lett.* **6**, 1479 (2006).

<sup>43</sup>Y. Huang, X. Duan, Q. Wei, and C. M. Lieber, *Science* **291**, 630 (2001).

<sup>44</sup>R. S. McLean, X. Huang, C. Khrpin, A. Jagota, and M. Zheng, *Nano Lett.* **6**, 55 (2006).

<sup>45</sup>R. Krupke, F. Hennrich, H. v. Löhneysen, and M. M. Kappes, *Science* **301**,

- 344 (2003).
- <sup>46</sup>R. Krupke, S. Linden, M. Rapp, and F. Hennrich, *Adv. Mater. (Weinheim, Ger.)* **18**, 1468 (2006).
- <sup>47</sup>N. Rozlosnik, M. C. Gerstenberg, and N. B. Larsen, *Langmuir* **19**, 1182 (2003).
- <sup>48</sup>B. S. Ong, Y. Wu, P. Liu, S. Gardner, and B. Chiang, *Adv. Mater.* **17**, 1141 (2005).
- <sup>49</sup>R. A. Street, *Nat. Mater.* **5**, 171 (2006).
- <sup>50</sup>R. J. Kline, M. D. McGehee, and M. F. Toney, *Nat. Mater.* **5**, 222 (2006).
- <sup>51</sup>R. Martel, T. Schmidt, H. R. Shea, and P. Avouris, *Appl. Phys. Lett.* **73**, 2447 (1998).
- <sup>52</sup>G. Zhang, P. Qi, X. Wang, Y. Lu, X. Li, R. Tu, S. Bangsaruntip, D. Mann, L. Zhang, and H. Dai, *Science* **314**, 974 (2006).
- <sup>53</sup>A. Colli, A. Fasoli, P. Beecher, P. Servati, S. Pisana, Y. Fu, A. J. Flewitt, W. I. Milne, J. Robertson, C. Ducati, S. De Franceschi, S. Hofmann, and A. C. Ferrari, *J. Appl. Phys.* **102**, 034302 (2007).